Detectability of Nonlinear Gravitational Wave Memory

Darin C. Mumma[1]
Mentors: Alan J. Weinstein[2], Colm Talbot[2], and Alvin K. Y. Li[2]
[1]*Departments of Physics and Philosophy, Grove City College, Grove City, PA 16127, US and*
[2]*LIGO Laboratory, California Institute of Technology, Pasadena, CA 91125, US*
(Dated: June 1, 2020)

Gravitational waves incident on a detector causes permanent distortion typically on the order of 10^{-23}-Hz$^{-1/2}$, the so-called memory effect. Linear and nonlinear components exist in gravitational wave memory, the latter appearing as a non-oscillatory, cumulative signal. Current gravitational wave detectors are unable to reliably detect and isolate this low-frequency, nonlinear component which skews the numerical inferences of gravitational wave source parameters. Because this effect is cumulative, it is non-negligible, and its non-oscillatory nature distinguishes it from the rest of the waveform, making it detectable, in theory. Though previous studies have quantified and suggested improvements for the detectability of nonlinear memory, more templates and new data are available than ever before. In this project, we apply Bayesian parameter estimation to simulated compact binary coalescences with injected memory to determine nonlinear memory detectability.

I. INTRODUCTION

Although all accelerating masses radiate gravitational waves, compact binary coalescences – binary systems consisting of black holes and/or neutron stars – are especially interesting because they emit the most detectable gravitational wave signals and many of their properties are known. Indeed, the amplitude and phase of a gravitational wave encodes source features such as mass, angular momentum, and location. The traditional waveform sourced from a compact binary coalescence is an oscillatory traveling wave with increasing frequency and momentary peak corresponding to the merger phase. As it propagates through spacetime, this waveform distorts surrounding mass arrangements in an oscillating pattern, but afterwards each arrangement returns to its original geometry. However, general relativity predicts that after a gravitational wave passes a truly free-falling arrangement of masses, a memory effect occurs in which a permanent nonzero difference in deformation is observable [1–3]. Further, all gravitational waves produce both linear and nonlinear memory.

Linear memory arises from non-oscillating masses and, thus, usually appears only in systems with hyperbolic orbits, neutrino ejection, or gamma-ray bursts [4]. Nonlinear memory arises from the signal contribution of secondary gravitational waves sourced by the initial wave emission. Unlike non-oscillating masses, secondary gravitational wave production occurs in many compact binary coalescences, making nonlinear memory especially prominent. Also, nonlinear memory accumulates over time because it is *hereditary* – depends on the entire past motion of the source. The non-oscillating and cumulative nature of nonlinear memory should, in theory, make it easy to distinguish from the primary component of a gravitational wave signal [5]. In practice this is not the case.

There is one reason why nonlinear memory is, in fact, hard to detect in a gravitational wave signal. As seen in Figure (1), the noise curves for the Livingston and Hanford detectors are minimized between 10–1000-Hz, the typical operating frequency of these detectors. However, nonlinear memory is all below this frequency band, where control and Poisson noise dominate. This has long been thought to lower the single-to-noise ratio of the memory effect below the resolution of the detectors.

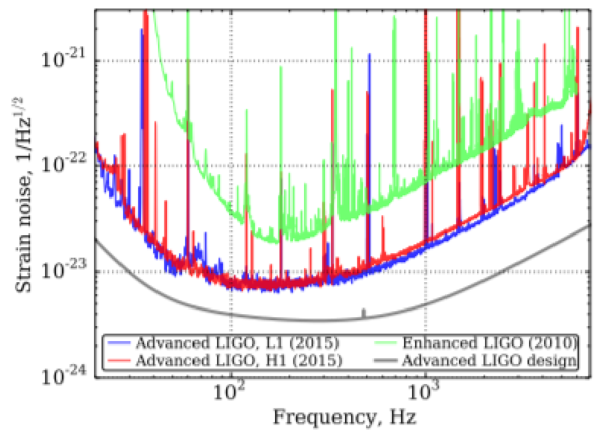

Figure 1. The noise curves for the LIGO Livingston detector and the LIGO Hanford detector during the first observing run. Also shown is the noise level for the Advanced LIGO design and the initial detectors. Retrieved from Martynov *et al [6].*

Even in higher frequency bands detector data is very noisy. The primary goal of gravitational wave signal analysis is to distinguish actual signals from this background noise. All phases of compact binary coalescence-sourced waveforms are well-modeled using numerical simulations, allowing a template library to be constructed over a broad range of binary component masses and spins. Matched filtering can then be used to compare these templates with the data and determine the best fit. When nonlinear gravitational wave memory enters the picture, this same process can also be used to determine the detectability of the memory contribution by comparing the memory component in the template with measured memory.

From here, we discuss the theoretical background behind gravitational waves, matched filtering, nonlinear memory, and parameter estimation in Section II. In Section III, we summarize the procedure involved in determining memory detectability. Finally, Section IV features the work plan for the project.

II. BACKGROUND

A. Gravitational Wave Theory and Detection

An implication of Einstein's general relativity is that black holes, neutron stars, and other massive objects accelerating in spacetime generate traveling ripples known as gravitational waves [7]. Here we will discuss the speed and polarizations of gravitational waves as well as instruments and methods used to detect them.

1. *Speed of gravity*

General relativity predicts that gravitational waves propagate at the speed of light [7], and several measurements have been made to confirm this prediction using astrophysical observations. Most notably, Velten, Jimenez, and Piazza [8] used twenty-five years of orbital decay measurements for the Hulse-Taylor binary, and Abbott *et al* [9] used the difference in arrival time between GW170817 and GRB170817, both sourced from the same binary neutron star merger. The first experimenters were able to constrain gravity's speed to within 1% of c and the second were able to constrain it to within only 10^{-13}% of c.

2. *Gravitational wave polarizations and detectors*

Another prediction of general relativity is that passing spacetime ripples distort an arrangement of test masses in an oscillatory manner. The frequency and amplitude of the oscillations are related to the angular momentum and mass of the ripple's source, respectively [10]. A Michelson-Morley interferometer may be used to record these variations in spacetime strain: two arms are set perpendicular to one another, and a laser and beamsplitter are arranged at the intersection point as shown in Figure (2). The laser is fired through the beamsplitter, creating two beams which travel along each arm and return after reflecting from mirrors placed at the end of each arm. Both beam paths are aligned to recombine at a photodiode located at the output port of the beamsplitter. Before a gravitational passes through, the only phase difference which exists between both beams arises from the difference in arm length, which is carefully adjusted to produce destructive interference at the photodiode.

However, both arm lengths are changed oppositely to one another by a passing gravitational wave, altering the phase difference and, thus, combined intensity of the light incident on the photodiode. This intensity information may be translated to strain information which is given in Equation (1)

$$h_{ij}(t,\ \mathbf{r}) = \sum_{A=+,\times} e_{ij}^{A}(\hat{\mathbf{n}}) \int_{-\infty}^{+\infty} h_A(f) e^{-i2\pi f (t - \frac{\hat{\mathbf{n}}\cdot\mathbf{r}}{c})}\, dt. \qquad (1)$$

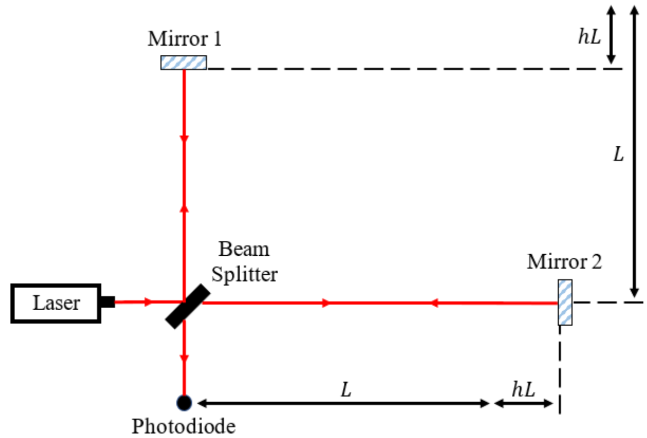

Figure 2. Simplified diagram of a standard LIGO detector. A gravitational wave traveling into the page is incident on the detector, changing each arm length by an amount hL (h is gravitational wave strain).

In general relativity, the spacetime metric is transverse-traceless gauge invariant, implying that free-falling test masses are at rest in spacetime. Although, the test masses (mirrors) in a given detector are supported by external forces, these are applied at low-frequencies (below 70–80-Hz), and are thus negligible at the operating frequencies of ground-based detectors. So, for these detectors, Equation (1) is independent of position $\mathbf{r}$, which may thus be set to 0 for a single detector (but will differ for other, non-collocated detectors). This yields the expression given in Equation (2)

$$h_{ij}(t) = \sum_{A=+,\times} e_{ij}^{A}(\hat{\mathbf{n}}) h_A(t), \qquad (2)$$

which clearly expresses the total strain as a sum of two polarization states, plus and cross. Both polarization states are transverse to the direction of propagation and are oriented 45° relative to one another as shown in Figure (3). Plus-polarized gravitational waves are a quarter-wave out of phase with cross-polarized gravitational waves, and, generally, incident gravitational waves are a linear combination of these two polarization states. Thus, gravitational waves may have linear, circular, or elliptical polarizations.

3. *Signal types and detection methods*

To date, there are multiple, known gravitational wave types including continuous, stochastic, burst, and compact binary coalescence gravitational waves. Continuous gravitational waves are radiated by spinning neutron stars and thus maintain constant frequency and amplitude. Stochastic gravitational waves likely come from especially distant sources and thus arrive from all directions, at all frequencies, and at all times. Burst gravitational waves have waveforms that are difficult to predict in advance but nevertheless exist as short duration pulses. Relevant to this paper, compact binary coalescence

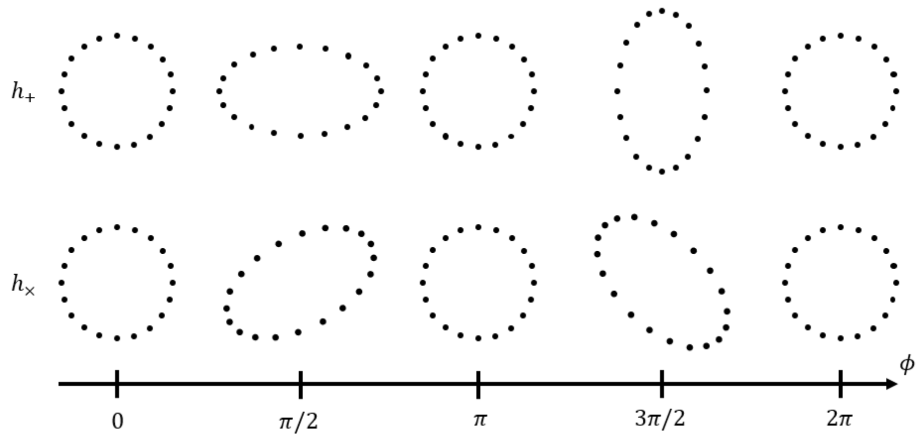

Figure 3. Linear polarizations of a gravitational wave illustrated over a complete phase cycle. Each dot represents a distinct test mass and the wave propagates into the plane of the paper.

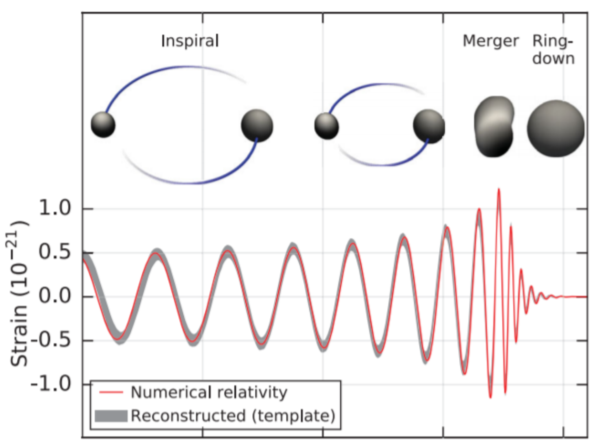

Figure 4. Compact binary coalescence gravitational-wave strain amplitude that shows the full bandwidth of a typical waveform. The inset images show the inspiral, merger, and ringdown phases of two coalescing black holes. Retrieved from Abbott *et al* [11].

gravitational waves are sourced from inspiraling compact objects, such as black holes and/or neutron stars, and thus vary in frequency and amplitude over time. Compact binary coalescences consist of three phases, including an inspiral, merger, and ringdown as shown in Figure (4). In the inspiraling stage, the separation distance and orbital period of the binary components decay due to radiated energy in the form of gravitational waves. This portion of the signal increases in frequency and amplitude as the merger approaches. In the merger phase, the signal's amplitude briefly peaks as the binary components combine. In the ringdown stage, the resulting merged black hole (or heavy neutron star) stabilizes, producing a signal with decreasing frequency and amplitude. Among these four types of gravitational waves, compact binary coalescence gravitational waves have the most well-modeled waveforms.

Increased detector sensitivity is achieved by equally extending both beam paths through the careful arrangement of mirrors which allow multiple reflections to take place before the beams are recombined. As a result, typical detector sensitivity allows for measurements of strain on the order of 10^{-22}-$\mathrm{Hz}^{-1/2}$. However, this high sensitivity to spacetime strain makes it hard to distinguish between gravitational wave signals and background noise. This noise is often both local and non-local, frequently masking or even mimicking gravitational wave signals. Random noise is due to local causes and is thus uncorrelated among an array of distant detectors, whereas a passing gravitational wave is incident on every point of the earth nearly simultaneously. So, using this *coincidence criterion*, comparison of data among multiple detectors may be used to distinguish real signals from random signals. However, non-local events such as earthquakes, and seismic waves (such as those caused by ocean waves colliding with the continental plates) may also be picked up by the detector and cannot be removed by comparison of multiple detector's data. Instead, such noise is identified and extracted by comparing real time data from seismographs and microphones to LIGO's data. Additional methods to reduce noise and increase detector sensitivity is shown in Figure (5). Identifying gravitational waves is further improved by comparing data to numerical templates constructed according to general relativity. This process, known as matched filtering, is explained in the next section.

B. Matched Filtering

The specifics of parameter estimation in determining memory detectability is mostly matched filtering. Here we will start by describing this process without memory and then include memory afterwards.

1. Matched filtering without memory

The ability to extract a signal from background noise is given by the signal-to-noise ratio, ρ, which is typically low,

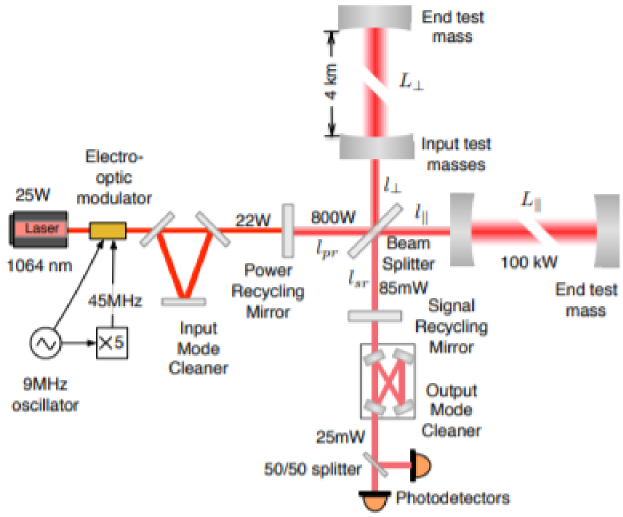

Figure 5. More detailed diagram of a standard LIGO detector. The annotations show the optical power in use during the first LIGO observing run. These power levels are a factor of ~8 smaller compared to the designed power levels. The Nd:YAG laser, with wavelength $\lambda = 1064$-nm, is capable of producing up to 180-W, but only 22-W were used. A suspended, triangular Fabry-Perot cavity serves as an input mode cleaner to clean up the spatial profile of the laser beam, suppress input beam jitter, clean polarization, and to help stabilize the laser frequency. The Michelson interferometer is enhanced by two 4-km-long resonant arm cavities, which increase the optical power in the arms by approximately a factor of 270. Since the Michelson interferometer is operated near complete destructive interference, all but a small fraction of the light is directed back towards the laser. The power recycling mirror resonates this light again to increase the power incident on the beamsplitter by a factor of nearly 40, improving the quantum Poisson noise sensing limit and filtering laser noises. On the anti-symmetric side, the signal recycling mirror is used to broaden the response of the detector beyond the linewidth of the arm cavities. An output mode cleaner is present at the antisymmetric port, to reject unwanted spatial and frequency components of the light, before the signal is detected by the main photodetectors. Retrieved from Martynov *et al [6]*.

and matched filtering is a process by which it may be maximized. In matched filtering, gravitational wave templates are cross-correlated with observed data in the frequency domain to see if the resulting amplitude spikes occur at the known frequencies contained in a given template. If the frequencies match, the parameters, identity, and waveform of the template source is taken to be those of the signal source as well. However, the overwhelming presence of noise in the data makes a direct application of this process impossible. First, a filter must be matched with each template to maximize the signal-to-noise ratio for all cross-correlations and is, in general given by Equation (3).

$$\tilde{K}(f) \propto \frac{\tilde{h}(f)}{S_n(f)}, \tag{3}$$

where $\tilde{K}(f)$ is the filter kernel, $\tilde{h}(f)$ is the template's waveform in the frequency domain, and $S_n(f)$ is the one-sided power spectral density of the data's noise.

To apply a given template's filter kernel, the template's waveform is cross-correlated with data to maximize the signal-to-noise ratio. The cross-correlation is given in Equation (4)

$$\hat{s} \propto \int \tilde{s}(f)\tilde{K}(f)\,df, \tag{4}$$

where $\tilde{s}(f)$ is the data's waveform in the frequency domain and $\hat{s}$ is related to ρ. Formally, $\rho = S/N$,where S is the expectation value of $\hat{s}$ when a signal is present, and N is the root mean square value of $\hat{s}$ when no signal is present. So, the goal is to select a $\tilde{K}(f)$ which maximizes Equation (4) across the signal's frequency band, maximizing ρ. Combining this selection process with the fact that a one-to-one correlation exists between filter kernels and template waveforms, identifying and characterizing gravitational wave signals is identical to determining which template maximizes the data's signal-to-noise ratio.

In practice, two nuances with the matched filtering process should be considered. Firstly, since the presence and waveform of a gravitational wave signal are unknown prior to the matched filtering process, the noise is often difficult to characterize. But ρ depends on S and N, and thus requires knowledge of the signal and background noise. Secondly, template banks are necessarily discrete, making even correctly-chosen templates an approximation and thus lowering ρ from its ideal value. Consequently, a threshold ρ must be set below a given template's ideal ρ, and a template which achieves values above this threshold identifies and characterizes the hidden gravitational wave. This process is enhanced by combining data from multiple detectors to increase ρ as given in Equation (5)

$$\rho_{net} = \sqrt{\sum_i \rho_i^2}, \tag{5}$$

where i runs over each detector and ρ_{net} is referred to as the network signal-to-noise ratio. Additionally, requiring each ρ_i to be above a certain threshold constitutes the coincidence criterion mentioned above and drastically reduces the likelihood of false detection.

2. *Matched filtering with memory*

Matched filtering can also be used to determine the detectability of the memory contribution. If the output of the matched filter using a template containing memory yields a significantly higher signal-to-noise ratio from the data than the output using a template without memory, the ability to detect memory is likely. The mathematical details involve parameter estimation and computation of a Bayes' factor, which will be explained after a discussion of nonlinear memory.

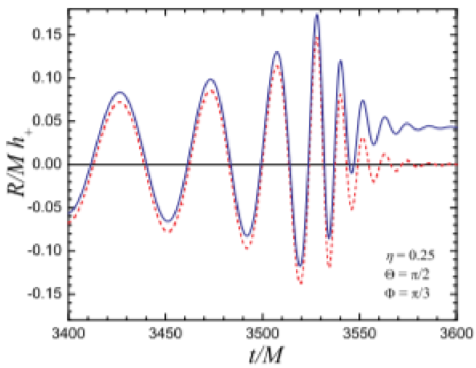

Figure 6. An example of a gravitational-waveform with memory. Shows the $+$ polarization for an equal-mass binary black hole coalescence with (blue) and without (red) the nonlinear memory. Retrieved from Favata [5].

C. Nonlinear Memory Theory

The nonlinear (Christodoulou) gravitational wave memory is a permanent displacement of freely-falling test masses due to the passage of gravitational waves [4, 5]. According to general relativity, a post-Newtonian expansion exists in which nonlinear memory is described by terms which immediately follow the primary waveform and linear memory. However, far from being negligible, these terms accumulate memory over the duration of the signal, increasing most rapidly during the merger as seen in Figure (6). These increasing terms arise from the signal contribution of secondary gravitational waves sourced by the primary waveform, and can thus be viewed as linear memory from waves which began from an arbitrary point in spacetime. Comparison between memory with and without a nonlinear component is shown in Figure (7) for plus and cross polarized signals and across a variety of mass and spin combinations. In most combinations, the non-linear component is readily seen to be substantial.

The strength of nonlinear memory depends on incident angle in much the same way as the primary waveform and, as just mentioned, increases monotonically over time. It is clear, then, that nonlinear memory has an angular and temporal dependence which vary independent of one another, suggesting separation of variables. Indeed, through an application of separation of variables and projection of the linear polarizations of the waveform onto the spherical harmonics, one yields

$$\delta h_{lm} = \frac{R}{4\pi c}\Gamma_{lm}^{l_1 l_2 m_1 m_2}(\Omega) H_{l_1 l_2 m_1 m_2}(T_0, T_F), \qquad (6)$$

where l and m designate a spherical harmonic mode for each binary component, δh_{lm} is the overall non-linear memory for a given mode, $\Gamma_{lm}^{l_1 l_2 m_1 m_2}(\Omega)$ encodes the angular dependence of the memory, and $H_{l_1 l_2 m_1 m_2}(T_0, T_F)$ encodes the time dependence. $\Gamma_{lm}^{l_1 l_2 m_1 m_2}(\Omega)$ is a geometry factor closely related to the spherical harmonics and may thus be tabulated and inserted in advance before any experiment-specific calculations are made. $H_{l_1 l_2 m_1 m_2}(T_0, T_F)$ is closely related to the total intensity of the secondary waveforms and thus must be computed after each signal is collected and processed. Using Equation (6), a tabulation of the spherical harmonics, and a properly chosen region of interest in an incident signal, nonlinear memory may be calculated.

Accurate identification and measurement of nonlinear memory will allow comparison with models, potentially lending further support to general relativity. Also, this will allow non-linear memory to be extracted from gravitational waveforms which will increase the accuracy of source parameter measurements. With the recent conclusion of the third LIGO observing run, much current data is now available, allowing for the detectability of non-linear memory to be determined. From such a determination, the magnitude and nature of sensitivity improvements for each detector may be evaluated so non-linear memory can be effectively detected in future observing runs.

D. Bayesian Parameter Estimation

Let the hypothesis H be the statement, “non-linear memory is present in the detector’s data” and, further, let D be the detector’s data. Then, $P(H \mid D)$ is the probability that non-linear memory is present in the data given the data we have at hand, $P(D \mid H)$ is the likelihood that we will detect nonlinear memory given that nonlinear memory is, in fact, present, $P(H)$ is the belief we have in the presence of nonlinear memory on the basis of prior information (or lack of information) alone, and $P(D)$ is the evidence offered by the data independent of the hypothesis under consideration. Bayes’ Theorem relates these four quantities as shown in Equation (7).

$$P(H \mid D) = \frac{P(D \mid H) \times P(H)}{P(D)} \qquad (7)$$

Equation (7) is used in Bayesian inferencing to update $P(H \mid D)$ as more data becomes available, and although we would eventually like to satisfy Equation (7) by determining $P(H \mid D)$ and $P(\sim H \mid D)$ and computing the associated Bayes’ factor, our present concern is finding $P(D \mid H)$ through parameter estimation.

The first step in parameter estimation is to present H as in Equation (8)

$$h_{tot} = h + \lambda h_{mem}, \qquad (8)$$

where h_{tot} is the total signal, h is the non-memory portion of the signal, and h_{mem} is nonlinear memory. Then, for a template with known memory $\lambda = P(H)$ and is thus 1, but for the same template superposed on noise, $\lambda = P(D \mid H)$ and can take on any value. The value of this second λ is the memory detectability and values close to 1 indicate a high likelihood of memory detection.

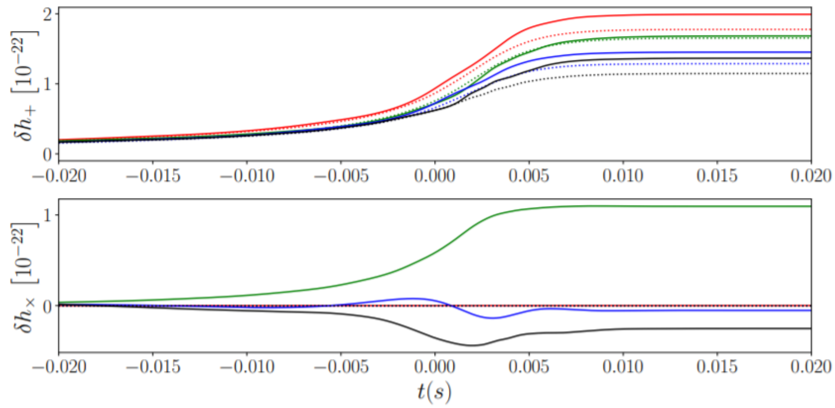

Figure 7. Including non-linear terms significantly affects the predicted memory. Comparison of the + (top panel) and × (bottom panel) polarizations of the memory time series when using only linear memory (dotted) and when using both linear and nonlinear memory (solid). The colors are for binaries as follows: red is equal-mass with non-spinning components, green is equal-mass with precessing spins, blue is unequal mass with non-spinning components, black is unequal mass with precessing spins. In all cases, the late-time memory is different by at least 10% compared with the linear memory-only case and is larger for large mass ratios and precessing spins. Retrieved from Talbot *et al* [12].

III. PROCEDURE

In this project, we will assess the detectability of memory in gravitational waves and subsequently search for methods to improve it. To achieve this goal, sufficient mastery of Bayesian parameter estimation, signal simulation, and python coding must be achieved. Here we will discuss the projected stages of the project.

Firstly, the primary author will become familiar with python and PyCBC [13, 14], a python package containing algorithms that can detect coalescing compact binaries and measure gravitational wave parameters. General python competency will equip him with the required coding skills which will be necessary later in the project while PyCBC will acquaint him with the general shape of gravitational waveforms and how to generate them.

Secondly, the primary author will become familiar with the python package GWmemory [15], which calculates and constructs nonlinear memory waveforms from selected gravitational signals. Familiarity with this package will improve his understanding of memory effects on gravity wave signals and how to generate signals with memory.

Third, the primary author will acquire a better understanding of Bayesian inference and become familiar with BILBY [16, 17], a python package which consists of inferencing tools for parameter estimation.

Fourthly, we will work on our primary goal by assessing the detectability of memory in gravitational waves. Equation (8) presents an all-or-nothing waveform model for templates, where λ represents the memory constant. We will superpose a signal with memory (i.e. $\lambda = 1$) on a typical noise distribution, and then apply matched filtering to measure the signal and infer the value of the memory constant. This inferred value represents the memory detectability, and a value close to 1 means we are likely able to identify memory in a given signal.

Fifthly, given additional time, we will investigate methods by which the detectability of gravitational wave memory can be improved.

IV. WORK PLAN

A work plan has been included in Table I, listing weekly project goals for the Summer 2020 LIGO SURF project.

[1] Y. B. Zeldovich and A. G. Polnarev. *Sov. Astron.*, 18(17), 1974.
[2] V. B. Braginsky and L. P. Grishchuk. *Sov. Phys. JETP*, 62(3): 427–430, 1985.
[3] V. B. Braginsky and K. S. Thorne. *Nature*, 327(6118):123–125, 1987.
[4] Kip S. Thorne. *Phys. Rev. D*, 45(2):520–524, 1992.
[5] M. Favata. *Classical Quantum Gravity*, 27(8), 2010.
[6] D. V. Martynov et al. *Physical Review D*, 93(11), 2016.
[7] A. Einstein. *Sitzungsber. Preuss. Akad. Wiss.*, 1:135–149, 1918.
[8] Hermano Velten, Jose Beltran Jimenez, and Federico Piazza. *International Journal of Modern Physics: Conference Series*, 45, 2017.
[9] B. P. Abbott et al. *The Astrophysical Journal*, 848(2):L13, 2017.
[10] B. P. Abbott et al. *Phys. Rev. X*, 9(3), 2019.
[11] B. P. Abbott et al. *Phys. Rev. Lett.*, 116(6), 2016.
[12] C. Talbot et al. *Phys. Rev. D*, 98(6), 2018.
[13] https://iopscience.iop.org/article/10.1088/0264-9381/33/21/215004/meta.
[14] https://pycbc.org/.
[15] https://github.com/colmtalbot/gwmemory.

Table I. Work plan for the Summer 2020 LIGO SURF program. Schedule is broken down by week and projected progress.

Date	Progress
June 1	1. Deadline for submitting project proposal.
June 16	2. Start of LIGO SURF 2020.
June 16–20 (Week 1)	3. Understand basic python and PyCBC functionality.
June 21–27 (Week 2)	4. Increase ability to work with PyCBC.
July 28–July 4 (Week 3)	5. Continue working with PyCBC and begin familiarizing with GWmemory.
July 5–11 (Week 4)	6. Continue familiarizing with GWmemory. 7. Submit interim report 1.
July 12–18 (Week 5)	8. Begin learning BILBY.
July 19–25 (Week 6)	9. Continue learning BILBY and start main project.
July 26–August 1 (Week 7)	10. Main Project: Formation of effective work flow. 11. Submit interim report 2. 12. Submit abstract.
August 2–8 (Week 8)	13. Main Project: Produce results.
August 9–15 (Week 9)	14. Investigate detectability improvement.
August 16–21 (Week 10)	15. Continue investigating detectability improvement. 16. Final presentation.
September 28	17. Deadline for submitting final report.

[16] https://lscsoft.docs.ligo.org/bilby/index.html.
[17] https://arxiv.org/abs/1811.02042.